Charge oscillations and interaction between potassium adatoms on graphene studied by first-principles calculations

Xiaojie Liu, Cai-Zhuang Wang, Hai-Qing Lin, Kai Chang, Jian Chen, and Kai-Ming Ho

Phys. Rev. B **91**, 035415 — Published 13 January 2015

DOI: 10.1103/PhysRevB.91.035415

Charge oscillation and interaction between potassium adatoms on graphene by first-principles calculations

Xiaojie Liu[1,2,§], Cai-Zhuang Wang[2,*], Hai-Qing Lin[1], Kai Chang[3,#] and Jian Chen[3,4], and Kai-Ming Ho[2]

[1]*Beijing Computational Science Research Center, Beijing, 100084, P. R. China*
[2]*Ames Laboratory-US Department of Energy, and Department of Physics and Astronomy, Iowa State University, Ames, Iowa, 50011, USA*
[3]*SKLSM, Institute of Semiconductors, Chinese Academy of Science, Beijing, 100083, China*
[4]*School of Physics and Nuclear Energy Engineering, Beihang University, Beijing 100191, China*

Abstract

Interaction between K adatoms on graphene is investigated by first-principles calculations based on density function theory and analytical analyses based on the **k**•**p** perturbation theory. The calculation shows that there is a strong repulsion between K adatoms. The main origin of this strong repulsion is not from the dipole-dipole interaction as suggested for K adatom on graphite surface, but comes from the screened Coulomb interaction. Potassium adatom on graphene donates its *s* electron and becomes K^+. The positively charged K adatom induces electron density oscillation on graphene which is responsible for the screened Coulomb repulsion between the K adatoms.

PACS numbers: 68.65.Pq, 68.43.Fg, 71.15.Mb, 68.55.Ln

§ xiaojie@csrc.ac.cn
* wangcz@ameslab.gov
# kchang@semi.ac.cn

Coulomb impurity in graphene is a problem of fundamental interest due to the unique electronic structure of graphene. Because graphene has linear energy dispersion and very small density-of-states around the Fermi level and consists of two sub-lattices, the electronic structure and transport properties of graphene are very sensitive to impurities [1-8]. Understanding and manipulating the interaction among the Coulomb impurities and between the impurity atoms and carbon atoms on graphene provide an effective approach for engineering the electronic structures to meet various requirements in the application of graphene.

While it is well-known that Coulomb or magnetic impurities on metal surface induce interesting phenomena such as Friedel oscillation in electron density thus the indirect interaction between the impurities, interaction between such impurities on graphene has not been well understood. It has been proposed that oscillation of the charge density induced by a charged impurity on graphene has a faster ($\delta\rho \sim r^{-3}$) decay than that in conventional 2D electron systems which decay as r^{-2} [5, 7]. Calculations based on tight-binding models suggested that in addition to the long wavelength Friedel oscillation, a short wavelength modulation of electron density also emerges due to the two sub-lattices on graphene [4, 9]. Energy-resolved maps of the local density-of-states by using STM also reveal electron density modulations on two different length scales, reflecting both intravalley and intervalley scattering [8]. Despite of intensive studies, our understanding of the behavior of charge oscillation and especially impurity interactions on graphene is still far from being completed. Most of the previous theoretical studies are based on model Hamiltonians, a fully self-consistent first-principles calculation is highly desirable and can provide useful insight for a better understanding of the mechanism of impurities on graphene.

In this paper, we performed first-principles calculations and analytical analyses based on the **k•p** perturbation theory to study the interaction between K adatoms on graphene and characterize the electron density oscillation behavior induced by the K adatoms. Potassium on graphene is chosen because alkali metal adatoms on graphene or graphite provides a prototype system for studying electron screening and Coulomb impurity interactions in two dimensions. Alkali metal-graphene system is also a topic

of great interest in device application and in the structural phase transition when alkali metal growth on graphene. Such a system has been a subject of intensive experimental and theoretical interest over the past twenty years [10-16]. Nevertheless, the nature of alkali metal interactions on graphite or graphene is still under much debate. For example, while Ref. [10] attributed the repulsions between K adatoms to the dipole-dipole interaction induced by charge transfer, Ref. [15] demonstrated that the interaction between Cs adatoms on graphene originates from a long-range repulsive Coulomb interaction. Our studies provide clean evident that the major contribution to the interaction between the K adatoms can be attributed to the screened Coulomb interaction. K adatoms donate their valence electrons to graphene and induce oscillation of electron density on graphene which is responsible for the screened Coulomb interaction. The findings from our study are useful for understanding the electron screening mechanism in graphene and the interactions controlling the assembly of metal nanostructures on graphene for future device applications.

The first-principles calculations are performed using the density functional theory (DFT) with generalized gradient approximation (GGA) in the form of PBE [17] implemented in the VASP code [18,19], including spin polarization and dipole moment corrections [20,21]. Valence electrons are treated explicitly and their interactions with ionic cores are described by projector augmented wave pseudopotentials [22,23]. The adatoms/graphene system is modeled by having two K adatoms at different separations on a 10×10 graphene supercell with periodic boundary conditions. The dimension of the supercell in the z direction is 15 Å which allows a vacuum region of about 12 Å to separate the atoms and their replicas in the z direction. The wave functions are expanded in a plane wave basis set with an energy cutoff of 600 eV. A k-point sampling of 2×2×1 Monkhorst-Pack grids in the first Brillouin zone and a Gaussian smearing with a width of σ=0.05 eV are used in the calculations. All atoms in the supercell are allowed to relax until the forces on each atom are smaller than 0.01 eV/Å. The supercell dimensions are kept fixed during the relaxation.

We first calculate the interaction energy between the two K adatoms on

graphene as the function of the separation distance between the two adatoms. The interaction energy is defined as $E_{inter}(r)=E_{a2}(r)-2E_{a1}$. Here, $E_{a2}(r)$ is the adsorption energy of two K adatoms on graphene at separation *r* and E_{a1} is the adsorption energy of a single K adatom. **Fig. 1** shows the $E_{inter}(r)$ (blue solid circles and blue solid line) as the function *r* between the two K adatoms. It is interesting to note that the interaction between K-K adatoms is repulsive for all the separation distances larger than 4.92 Å. The repulsive interaction energy between two K adatoms is about 0.6 eV which is significant.

We note that in a recent paper [10], repulsive interaction between potassium adatoms on graphite has been observed by STM experiment and molecular dynamics simulations. It was proposed that such repulsive interactions are mainly due to long-range electric dipole-dipole interaction resulted from the significant charge transfer from K adatoms to graphite [9]. In order to see if the electric dipole-dipole interaction is responsible for the repulsion of K adatoms on graphene, we calculated the electric dipole moment and dipole-dipole interaction on graphene. We found that adsorption of K adatoms on graphene can induce electric dipole moment as large as 6.33 Debye per adatom as long as the separation distance between the two K adatoms is larger than 7.0 Å. At the smaller distance of 4. 92 Å, the electric dipole moment is about 3.40 Debye per adatom due to the overlap of wave functions between the two adatoms. Using the electric moments obtained from our calculations, we can estimate the contribution of the dipole-dipole interaction to the total interaction energy. Electric dipole-dipole interaction for two non-overlap dipoles perpendicular to the graphene layer and at a distance *r* is $V_d(r)=\frac{\alpha}{4\pi\varepsilon_0}\frac{\mu_1\mu_2}{r^3}$. Here μ_1 and μ_2 are the electric dipole moments on each K adatom, respectively. The value of α should be 1.0 if the two dipoles are in vacuum and 2.0 if on a metal surface due to the screening effect [18]. Since graphene is a two dimensional system and the density of free carrier is smaller than that on a metal surface, the screening effects would be weaker than that on metal surface and the value of α would be between 1.0 and 2.0. Using the electric dipole moments obtained from our first-principles calculations and α=1.5, the

dipole-dipole repulsive energy $E_{d\text{-}d}(r)$ as the function of distance r is also plotted in **Fig. 1** (red solid circles and red dot line). We found that $E_{d\text{-}d}(r)$ accounts for only a small fraction of the total interaction energy as seen in **Fig. 1**. Therefore, electric dipole-dipole interaction can only partially contribute to the repulsive interaction in this system but it is not the dominant one, at least at the interaction range studied in this paper.

Since K on graphene causes very little lattice distortion to the graphene, elastic interaction is expect to play a negligible role in the interaction energy. On the other hand, from the charge transfer analysis we found that in the very dilute adsorption limit as in the present case of study the outer shell *s* electrons of the K adatoms transfer completely to graphene upon adsorption and leave the K adatoms in K^+ states [24]. Therefore, strong repulsion between the two K adatoms on graphene can be attributed to Coulomb interaction. However, as shown in **Fig. 1**, although the repulsive interaction between the two K^+ is strong, it is much smaller than the bare Coulomb interaction (pink dash line in **Fig. 1**). This result indicates strong screening effect caused by the redistribution of the electrons on graphene due to the presence of the K^+ adatoms. We note that experiment in Ref. [15] also suggests strong Coulomb interaction between Cs adatoms on single layer or bi-layer of graphene since the interaction between Cs adatoms decay as a power law (~1/r).

In order to gain a better understanding of the screening and the interaction between the K adatoms, we have investigated the electron density redistribution induced by a K adatom on graphene by first-principles calculations. A 12×12 graphene supercell with periodic boundary conditions is used in order to see the electron density oscillation further away from the K adatom. Because the electron density on graphene is very small, in order to see the charge oscillation due to the K adatom adsorption more clearly, we calculated the change in the electron density $\Delta\rho(r)$ (we call it interaction electron density (IED) afterwards) due to the adatom-graphene interaction instead of total electron density. The IED $\Delta\rho(r)$ is defined as $\Delta\rho(r) = \rho(r) - (\rho_{gra}(r) + \rho_{ads}(r))$ where $\rho(r)$ is the charge density of the K/graphene

system, $\rho_{gra}(r)$ and $\rho_{ad}(r)$ are the charge densities of the pure graphene and the K adatom calculated separately. The $\Delta\rho(r)$ defined in this way accounts for the electron redistribution due to the interaction between K adatom and graphene. In **Fig. 2 (a)**, the top view of the 2D-contour of $\Delta\rho(r)$ in the plane through the graphene layer is plotted. The oscillation of $\Delta\rho(r)$ from the K adatom can be clearly seen from the plot. A quantitative measure of the oscillation and decay of $\Delta\rho(r)$ away from the K adatom is shown by the line scans in **Fig. 2 (b)**, **(c)** and **(d)** respectively. The line scans are along the arm-chair direction through carbon atoms (**Fig. 2(b)**) and zigzag direction through carbon atoms (**Fig. 2 (c)**) or carbon bonds (**Fig. 2(d)**) as indicated in **Fig. 2 (a)**. The line scans show clearly the oscillatory and decay behavior of the $\Delta\rho(r)$ away from the K adatom. The line scans also show that the details of the oscillation and decay are direction dependent but the oscillations in all directions have short wavelengths.

Electron density oscillation and screening effects induced by Coulomb impurities on graphene have recently attracted considerable theoretical interest [25-32]. It has been shown that a positively charged impurity on graphene induces short wavelength electron density oscillation due to the intervalley scattering in addition to the long wavelength Friedel oscillation due to the intravalley scattering. The decay of in electron density away from the impurity scales like r^{-3} instead of r^{-2} in 2D electron gas. A line scans of electron distribution from our first-principles calculation show that the peaks along the armchair direction in **Fig. 2 (b)** can be divided into three sets: those on sub-lattice carbon atom A (labeled A, i.e., pink solid circles), those on sub-lattice carbon atom B (labeled B, i.e., blue solid circles), and those between the two sub-lattice atoms (the rest, i.e., yellow solid circles). We can see electron charge on the atoms decay monotonically away from the impurity while electron density oscillated between the atoms. Similar behavior can also be seen from the line scans along the zigzag direction as one can see from **Fig. 2 (c)** and **(d)**. Overall the decay of the electron density away from the impurity is close to the theoretical prediction of $\sim r^{-3}$. The electron charge on the carbon atoms can also be seen from the Mullikan charge analysis using the QUAMBO method [33] as shown in **Fig. 2 (e)**. The decay of

the electron charge on the carbon atoms away from the K adatom from our Mullikan charge analysis is found to decay slightly fast than the r^{-3} as shown in **Fig. 2 (e)**.

We also performed analytical analyses based on the **k•p** perturbation theory to elucidate the origins of electron charge oscillation and screening induced by the K adatom adsorption. Unlike the previous studies, we examine the effects of the inter- and intravalley scattering separately to investigate the role played by the intervalley electron scattering on the screening which is mostly relevant to our present first-principles calculations. We obtain the analytical expression of the dielectric function for a system with a positive charged impurity on graphene in terms of inter and intravalley scattering separately:

$$\varepsilon_{intra} = 1 + \frac{e^2}{2\kappa\varepsilon_0 q}\frac{g_s g_v k_F}{2\pi\hbar v_F}\begin{cases} 1 & (q < 2k_F) \\ 1 - \sqrt{\frac{1}{4} - \frac{k_F^2}{q^2}} + \frac{\pi q}{8k_F} - \frac{q}{4k_F}\sin^{-1}\frac{2k_F}{q} & (q > 2k_F) \end{cases} \quad (1)$$

$$\varepsilon_{inter} = 1 + \frac{e^2}{2\kappa\varepsilon_0 \tilde{q}}\frac{g_s k_F}{2\pi\hbar v_F}\cos^2\theta_2\begin{cases} 0 & (q < 2k_F) \\ -\sqrt{\frac{1}{4} - \frac{k_F^2}{q^2}} - \frac{\pi q}{8k_F} + \frac{q}{4k_F}\sin^{-1}\frac{2k_F}{q} & (q > 2k_F) \end{cases} \quad (2)$$

where $g_s = g_v = 2$ denote the spin and valley degeneracy, $v_F = 10^6 m/s$ is the Fermi velocity of electron in graphene, $\tilde{q} = \sqrt{q^2 + Q^2 + 2qQ\cos\theta_2}$ and **Q** is the vector in the reciprocal lattice connecting the nearest neighbouring valleys K and K'. The detailed derivations about the dielectric function and the screened charge potential are given in the Appendix.

Figs. 3 (a) and **(b)** clearly shows that the intervalley scattering indeed introduce short wavelength charge oscillation with the period of several Angstroms. Interestingly, the Friedel oscillations also show significant anisotropic behavior along the zigzag and armchair directions. The screened Coulomb potentials are shown in **Figs. 3 (c)** and **(d)** in comparison with the unscreened bare potential. We can see that the screened potential is much weaker than the bare potential, consistent with our first-principles calculation results shown in **Fig. 1**. We can see from the **Figs. 3 (c)**

and **(d)** that the screening from the intervalley electron scattering plays an important role which gives a short-wavelength oscillation. Although the analytical results can explain the short-wavelength oscillation of electron density and screened Coulomb potential, one still can see the difference between the results obtained from the DFT calculation and the analytical expression from the **k•p** model. The former shows a more rapid oscillation than the latter. This difference may arise from the lacking of detailed treatment of the local field, charge transfer, lattice distortion near the adatoms in the **k•p** calculation. Another source for the discrepancy would be due to the neglecting of non-linear screening effects in the **k•p** model. It has been shown [34, 35] that linear screening would be inadequate at and close to the charge neutrality point which is relevant to the low K coverage situation studied in this paper.

In order to further validate the screened Coulomb interaction picture, we examined the effects of electron doping level on the interaction energy between the two K adatoms. We compare the interaction energies for two K adatoms on 8×8 and 10×10 graphene supercells respectively. For two K adatoms on a 8×8 graphene, the electron doping density is about 6.0×10^{-3} electron/Å^2. For two K adatoms on a 10×10 graphene, the electron doping density is ~3.8×10^{-3} electron/Å^2. As one can see from **Fig. 4**, the interaction energy for two K adatoms on 8×8 graphene is about 0.077 eV (or ~14.4%) smaller than that on 10×10 graphene at the K-K separation of 8 Å. This result demonstrates that the higher the electron doping level, the stronger the screening effects, further confirming our conclusion of screened Coulomb interaction between K adatoms on graphene.

As discussed above, a K adatom on graphene induces oscillatory electron redistribution. When the second K adatom is introduced, it will feel the screening rather than bare Coulomb interaction from the first K adatom. The repulsive interaction between the two K adatoms is therefore dominated by this screening Coulomb interaction. In fact, when the second adatom is added, it will also cause the redistribution of the electron on graphene such that its positive local charge can be effectively screened. The electron density oscillations induced by the two adatoms will meet each other and form an interfered wave. As shown in **Fig. 5**, the interaction charge

density $\Delta\rho(r)$ is dependent on the separation distance and the orientation of the two adatoms relative to the graphene substrate. From **Fig. 5**, one can see that if the separation distance is small (less than 10 Å), the two adatoms look like forming a pair of impurity and create the charge oscillation around the pair of adatoms. As the distance become large, the oscillation from each adatom becomes more independent. Analytic modeling the interference of the charge oscillation induced by two or more Coulomb impurities would be a very interesting future research.

In summary, we have studied the interaction between two K adatoms on graphene using first-principles calculations. We showed that the main contribution to the repulsion between the two K adatom is the strong screened Coulomb interaction rather than the dipole-dipole interaction proposed previously for potassium on graphite surface [10]. Short wave-length electron charge oscillation in graphene induced by the K adatom adsorption is also observed by the first-principles calculations. Analytical analyses based on the $\mathbf{k \cdot p}$ perturbation theory indicate that the electron screening is originated from the oscillation of the electron density in graphene. Our study provides useful insights into the mechanism of the screening and its relation to the charge oscillations in two-dimensional systems. Understanding the unique interactions between adatoms on atomically well-defined surfaces such as graphene also paves a way for controlling the assembly of metal nanostructures on two-dimensional substrates for future device applications.

Work at Ames Laboratory was supported by the US Department of Energy, Basic Energy Sciences, Division of Materials Science and Engineering, including a grant of computer time at the National Energy Research Scientific Computing Centre (NERSC) in Berkeley, CA under Contract No. DE-AC02-07CH11358. Xiaojie Liu also acknowledges the support by the National Natural Science Foundation of China under Grant No. 11204013 and the China Postdoctoral Science Foundation under Grant No. 2013T60056.

APPENDIX: Derivations of the dielectric function and the screened charge potential based on the k•p perturbation theory

To obtain the Friedel oscillations of the screened potential and charge density, we derive the static dielectric function ε(0, **q**) including the intervalley scattering process based on the low-energy continuum **k** · **p** Hamiltonian. Using the random phase approximation (RPA), the dielectric function is

$$\varepsilon(\omega,\mathbf{q}) = 1 - \upsilon(q)\sum_{\mathbf{k},ll'} \frac{[f_{\mathbf{k}} - f_{\mathbf{k}'}]F}{E_{l\mathbf{k}} - E_{l'\mathbf{k}'} + \hbar\omega + i0^{+}},$$

where $\upsilon(q) = e^2/2\varepsilon_0\kappa q$ is the bare Coulomb interaction component with κ is the background dielectric constant, $E_{l\mathbf{k}}$, $E_{l'\mathbf{k}'}$ denote the two subband dispersions with the band index $l, l' = \pm 1$, f is the Fermi-Dirac distribution function. The static dielectric function ε(0, **q**) is the zero-frequency limit $\omega \to 0$. We introduce the initial and final wave vectors $\mathbf{k}, \mathbf{k}'$ starting from the nearest Dirac points (**K** or **K**') and their directions $\phi_{\mathbf{k}}$, $\phi_{\mathbf{k}'}$. For the intravalley scattering, the form factor $F_{intra} = [1 + ll'\cos(\phi_{\mathbf{k}'} - \phi_{\mathbf{k}})]/2$. For the intervalley case, $F_{inter} = [1 - ll'\cos(\phi_{\mathbf{k}} + \phi_{\mathbf{k}'})]/2$. After a long tedious derivation, we represent both the intravalley and intervalley static dielectric functions with the transition wave vector $\mathbf{q} = \mathbf{k} - \mathbf{k}'$ and its orientation along θ_2 away from the reference direction connecting the two nearest neighboring valleys (see the inset of Fig. 3(a)),

$$\varepsilon_{intra} = 1 + \frac{e^2}{2\kappa\varepsilon_0 q}\frac{g_s g_v k_F}{2\pi\hbar v_F}\begin{cases} 1 & (q < 2k_F) \\ 1 - \sqrt{\frac{1}{4} - \frac{k_F^2}{q^2}} + \frac{\pi q}{8k_F} - \frac{q}{4k_F}\sin^{-1}\frac{2k_F}{q} & (q > 2k_F) \end{cases} \quad (1)$$

$$\varepsilon_{inter} = 1 + \frac{e^2}{2\kappa\varepsilon_0 \tilde{q}}\frac{g_s k_F}{2\pi\hbar v_F}\cos^2\theta_2\begin{cases} 0 & (q < 2k_F) \\ -\sqrt{\frac{1}{4} - \frac{k_F^2}{q^2}} - \frac{\pi q}{8k_F} + \frac{q}{4k_F}\sin^{-1}\frac{2k_F}{q} & (q > 2k_F) \end{cases} \quad (2)$$

where $g_s = g_v = 2$ denote the spin and valley degeneracy, $v_F = 10^6 m/s$ is the Fermi velocity in graphene, $\tilde{q} = \sqrt{q^2 + Q^2 + 2qQ\cos\theta_2}$ and **Q** is the vector in the reciprocal lattice connecting the nearest neighboring valleys **K** or **K**'.

Considering an charged impurity above the graphene at a distance *d*, the bare Coulomb potential, $Ze\delta(\mathbf{r})\delta(z-d)$, is screened by free electrons in graphene due to

the Coulomb interaction. This changes the bare Coulomb potential and results in an in-plane charge density oscillation. The screened potential V(**r**) is obtained form a Fourier transform

$$V(\mathbf{r}) = -\sum_{\mathbf{q}} \frac{Ze^2}{2\kappa\varepsilon_0 \varepsilon(0,\mathbf{q})} e^{-qd} e^{i\mathbf{q}\cdot\mathbf{r}}$$

The minus indicates an attractive potential for a positive external charge, and vice versa. The induced charge density fluctuation Δρ(**r**) can be calculated using Poisson's equation as

$$\Delta\rho(\mathbf{r}) = Ze\sum_{\mathbf{q}} \left[1 - \frac{1}{\kappa\varepsilon(0,\mathbf{q})}\right] e^{-qd} e^{i\mathbf{q}\cdot\mathbf{r}}$$

Considering the intervalley scattering and the sixfold rotational symmetry in graphene, we obtain the final expressions of V(**r**) and Δρ(**r**) for further numerical calculations,

$$\begin{aligned} V(\mathbf{r}) = & -\frac{Ze^2}{2\kappa\varepsilon_0}\frac{1}{4\pi^2}\int_0^{\pi}\int_0^{q_m^{intra}} \left[\frac{1}{\varepsilon_{intra}} - 1\right] \frac{J_{intra}}{q} \cdot q \cdot \mathrm{d}q\mathrm{d}\theta \\ & -\frac{Ze^2}{2\kappa\varepsilon_0}\frac{1}{4\pi^2}\int_0^{\pi}\int_0^{q_m^{inter}} \left[\frac{1}{\varepsilon_{inter}(\theta_2)} - 1\right] \frac{J_{inter}}{\tilde{q}} \cdot q \cdot \mathrm{d}q\mathrm{d}\theta_2 \\ & + V_0(r) \end{aligned}$$

where $V_0(r) = -Ze^2 / 4\pi\kappa\varepsilon_0\sqrt{r^2 + d^2}$ is the bare Coulomb potential, and

$$\begin{aligned} \Delta\rho(\mathbf{r}) = & \frac{Ze}{4\pi^2}\int_0^{\pi}\int_0^{q_m^{intra}} \left[1 - \frac{1}{\kappa\varepsilon_{intra}}\right] J_{intra} \cdot q\mathrm{d}q\mathrm{d}\theta \\ & + \frac{Ze}{4\pi^2}\int_0^{\pi}\int_0^{q_m^{inter}} \left[1 - \frac{1}{\kappa\varepsilon_{inter}}\right] J_{inter} \cdot q\mathrm{d}q\mathrm{d}\theta_2 \end{aligned}$$

where $J_{intra} = 2\cos(qr\cos\theta)e^{-qd}$, $J_{inter} = 2[J(\theta_2) + J(-\theta_2)]e^{-\tilde{q}d}$ and

$$\begin{aligned} J = & \cos(Qr\cos\theta_0 + qr\cos(\theta_2 - \theta_0)) \\ & + \cos(Qr\cos(\theta_0 - \pi/3) + qr\cos(\theta_2 - \theta_0 + \pi/3)) \\ & + \cos(Qr\cos(\theta_0 - 2\pi/3) + qr\cos(\theta_2 - \theta_0 + 2\pi/3)) \end{aligned}$$

here θ is the angle between **q** and **r** and θ_0 is the orientation angle of **r**.

References

[1] W. Kohn and K. H. Lau, Solid State Comm., **18**, 553 (1976).

[2] A. V. Shytov, D. A. Abanin, and L. S. Levitov, Phys. Rev. Lett., **103**, 016806 (2009).

[3] C. Bena, Phys. Rev. Lett., **100**, 076601 (2008).

[4] A. Bacsi and A. Virosztek, Phys. Rev. B, **82**, 193405 (2010).

[5] V. V. Cheianov, O. Syljuåsen, B. L. Altshuler, and V. I. Falko, Phys. Rev. B, **80**, 233409 (2009).

[6] S. Saremi, Phys. Rev. B, **76**, 184430 (2007).

[7] V. V. Cheianov and V. I. Falko, Phys. Rev. Lett., **97**, 226801 (2006).

[8] G. M. Rutter, J. N. Crain, N. P. Guisinger, T. Li, P. N. First, J. A. Stroscio, Science, **317**, 219 (2007).

[9] V. N. Kotov, B. Uchoa, V.M. Pereira, F. Guinea, A.H. Castro Neto, Rev. Mod. Phys. **84**, 1067 (2012).

[10] J. Renard, M. B. Lundeberg, J. A. Folk, and Y. Pennec, Phys. Rev. Lett., **106**, 156101 (2011).

[11] Z. Y. Li, K. M. Hock, and R. E. Palmer, Phys. Rev. Lett., **67**, 1562 (1991).

[12] F. Yin, J. Akola, P. Koshinen, M. Manninen, and R. E. Palmer, Phys. Rev. Lett., **102**, 106102 (2009).

[13] J. Algdal, M. Breitholtz, T. Kihlgren, S.-Å. Lindgren, and L. Walldén, Phys. Rev. B, **73**, 165409 (2006).

[14] C. Virojanadara, S. Watcharinyanon, A. A. Zakharov, and L. I. Johansson, Phys. Rev. B, **82**, 205402 (2010).

[15] C.-L. Song, B. Sun, Y.-L. Wang, Y.-P. Jiang, L. Wang, K. He, X. Chen, P. Zhang, X.-C. Ma, Q.-K. Xue, Phys. Rev. Lett., **108**, 156803 (2012).

[16] M. Caragiu and S. Finberg, J Phys.: Conden. Matt. **17**, R995 (2005).

[17] J. P. Perdew, K. Burke, and M. Ernzerhof, Phys. Rev. Lett., **77**, 3865 (1996).

[18] G. Kresse and J. Hafner, Phys. Rev. B, **47**, 558 (1993).

[19] G. Kresse and J. Furthmüller, Phys. Rev. B, **54**, 11169 (1996); Comput. Mater. Sci., **6**, 15 (1996).

[20] G. Makov and M. C. Payne, Phys. Rev. B, **51**, 4014 (1995).

[21] J. Neugebauer and M. Scheffler, Phys. Rev. B, **46**, 16067 (1992).

[22] P. E. Blöchl, Phys. Rev. B, **50**, 17953 (1994).

[23] G. Kresse and D. Joubert, Phys. Rev. B, **59**, 1758 (1999).

[24] The amount of electron transfer from K to graphene is dependent on the coverage of K adatoms. For a single K adatom on graphene, DFT calculations using a (4×4) unit cell (an equipollent coverage of 0.0625 ML), the charge transfer is about 0.6-0.7 e. Charge transfer from K to graphite has been measured by experiment to be 0.38 ± 0.11e at the K coverage between 0.17 and 0.30 ML [Ref 16]. However, when the unit cell is increased to (6×6) or larger, our calculations show that the charge transfer is 1.0 e by QUAMBO analysis or 0.9 e by Bader's analysis. For two K adatoms on a (10×10) graphene unit cell as used in the present calculation, the electron transfer from each K adatom is also about 1.0 e or 0.9 e from our QUAMBO or Bader's analysis respectively, as long as the separation between the two K adatoms is larger than 7 Å.

[25] V. M. Pereira, J. Nilsson, A. H. Castro Neto, Phys. Rev. Lett. **99**, 166802 (2007).

[26] A.V. Shytov, M.I. Katsnelson, L.S. Levitov, Phys. Rev. Lett. **99**, 236801 (2007).

[27] I. S. Terekhov, A.I. Milstein, V.N. Kotov, O.P. Sushkov, Phys. Rev. Lett. **100**, 076803 (2008).

[28] M. I. Katsnelson, Phys. Rev. B **74**, 201401(R) (2006).

[29] R. R. Biswas, S. Sachdev, D. T. Son, Phys. Rev. B **76**, 205122 (2007).

[30] M. M. Fogler, D.S. Novikov, B.I. Shklovskii, Phys. Rev. B **76**, 233402 (2007).

[31] Y. Wang, V.W. Brar, A.V. Shytov, Q. Wu, W. Regan, H.-Z. Tsai, A. Zettl, L.S. Levitov, M.F. Crommie, Nature Phys. **8**, 653 (2012).

[32] E. H. Hwang and S. Das Sarma, Phys. Rev. B, **75,** 205418 (2007).

[33] T. L. Chan, Y. X. Yao, C. Z. Wang, W. C. Lu, J. Li, X. F. Qian, S. Yip, K. M. Ho, Phys. Rev. B, **76**, 205119 (2007);X. F. Qian, J. Li, L. Qi, C. Z. Wang, T. L. Chan, Y. X. Yao, K. M. Ho, S. Yip, Phys. Rev. B, **78**, 245112 (2008);Y. X. Yao, C. Z. Wang, K. M. Ho, Phys. Rev. B, **81**, 235119 (2010).

[34] D. P. DiVincenzo and E. J. Mele, Phys. Rev. B **29**, 1685 (1984).

[35] M. I. Katsnelson, Phys. Rev. B **74**, 201401(R) (2006).

Figures Caption:

FIG. 1. Interaction energy E_{inter} (blue solid circles s and blue solid line) of K-K adatoms on graphene as a function of K-K separation. The electric dipole-dipole interaction $E_{d\text{-}d}$ (red solid circles and red dot line) and bare Coulomb interaction $E_{b\text{-}c}$ (pink dash line), respectively, are also shown for comparison.

FIG. 2. (a) The top view of the 2D-contour (color scale from -0.002 to 0.002 electrons/Å^3) the IED $\Delta\rho(r)$ in the plane through the graphene layer. (b) The line scans of $\Delta\rho(r)$ along the arm-chair directions in graphene as indicated in (a). (c) and (d) The line scans of $\Delta\rho(r)$ along the zigzag directions cutting through C atoms or C-C bonds respectively in graphene as indicated in (a). The intensities of the peaks in each direction can be fitted well to $\sim r^{-3}$ as indicated by solid green lines. The vertical dash lines in (b), (c) and (d) indicate the position of carbon atoms and C-C bonds respectively, in the armchair and zigzag directions in graphene. (e) Mullikan exceeded charges on sub-lattices A and B respectively as the function of the distance from the K adatom. The green line is $1.7\times r^{-3}$.

FIG. 3. The electron density variation as a function of the distance r along the zigzag (a) and armchair (b) directions, respectively. In (c) and (d), the screened Coulomb potentials along the above two directions are compared with the bare Coulomb potentials.

FIG. 4. Comparison of interaction energy between two K adatoms on 8×8 and 10×10 graphene. Graphene supercell with smaller size will have higher level of electron doping. Higher electron doping level in the smaller supercell results in smaller interaction energy due to stronger electronic screening.

FIG. 5. Interaction charge density $\Delta\rho(r)$ for two K adatoms on graphene (color scale from 0.00 to 0.008 electrons/Å^3). $\Delta\rho(r)$ is found to be dependent on the separation distance and the orientation of the two adatoms relative to the graphene substrate.

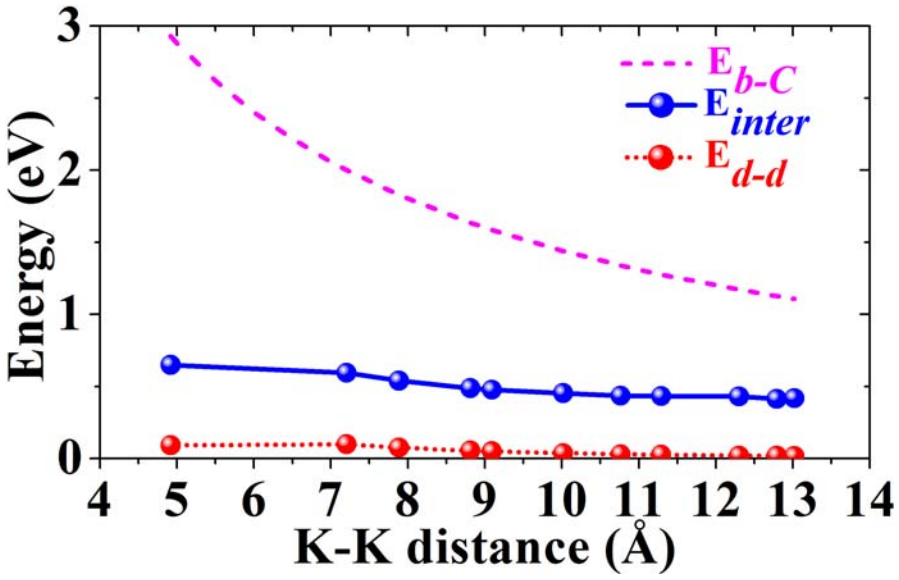

FIG. 1. Interaction energy E_{inter}(blue solid circles s and blue solid line) of K-K adatoms on graphene as a function of K-K separation. The electric dipole-dipole interaction E_{d-d} (red solid circles and red dot line) and bare Coulomb interaction E_{b-c} (pink dash line), respectively, are also shown for comparison.

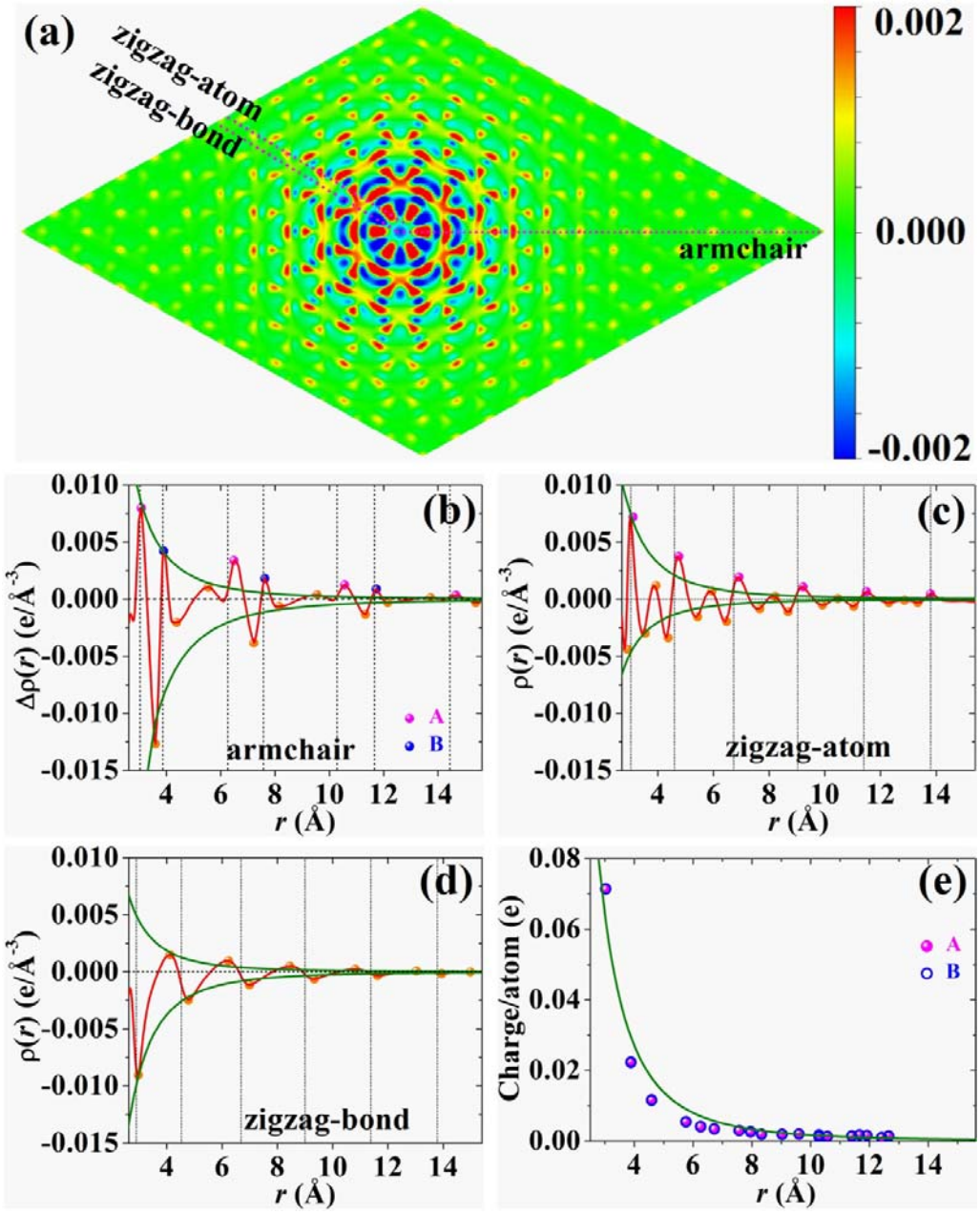

FIG. 2. (a) The top view of the 2D-contour (color scale from -0.002 to 0.002 electrons/Å^3) the IED $\Delta\rho(r)$ in the plane through the graphene layer. (b) The line scans of $\Delta\rho(r)$ along the arm-chair directions in graphene as indicated in (a). (c) and (d) The line scans of $\Delta\rho(r)$ along the zigzag directions cutting through atoms or C-C bonds respectively in graphene as indicated in (a). The intensities of the peaks in each direction can be fitted well to $\sim r^{-3}$ as indicated by solid green lines. The vertical dash lines in (b), (c) and (d) indicate the position of carbon atoms and C-C bonds respectively, in the armchair and zigzag directions in graphene. (e) Mullikan exceeded charges on sub-lattices A and B respectively as the function of the distance from the K adatom. The green line is $1.7\times r^{-3}$.

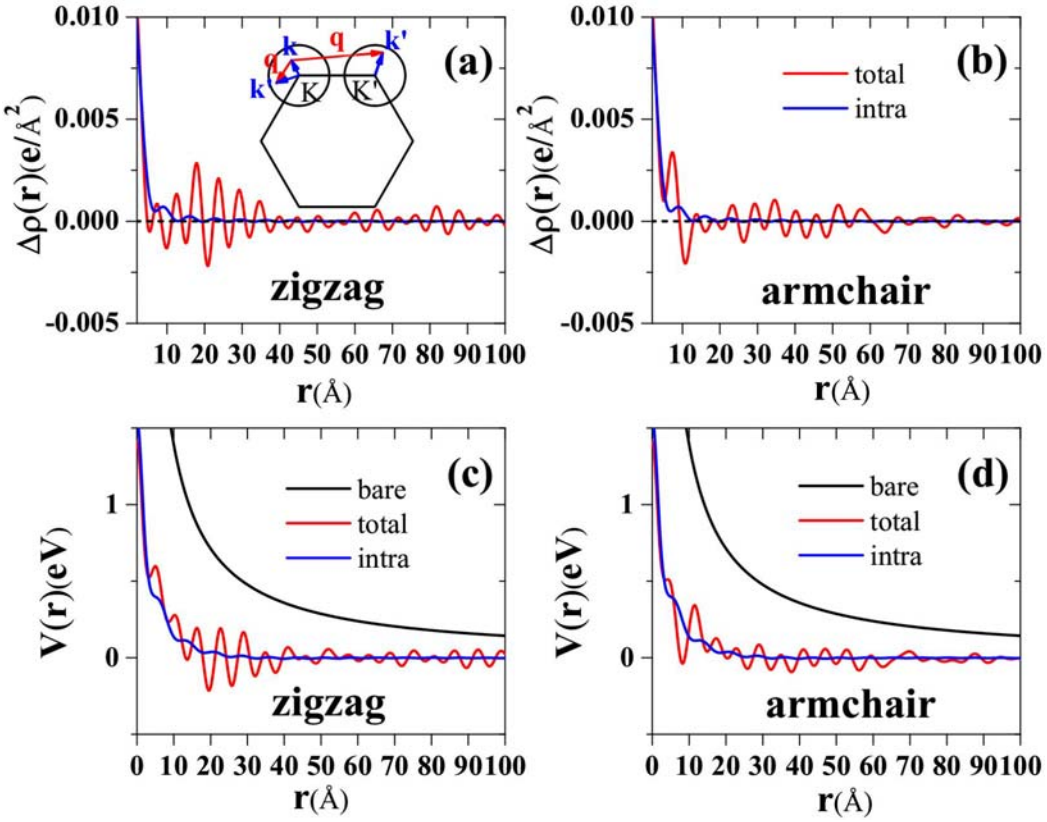

FIG. 3. The electron density variation as a function of the distance r along the zigzag (a) and armchair (b) directions, respectively. In (c) and (d), the screened Coulomb potentials along the above two directions are compared with the bare Coulomb potentials.

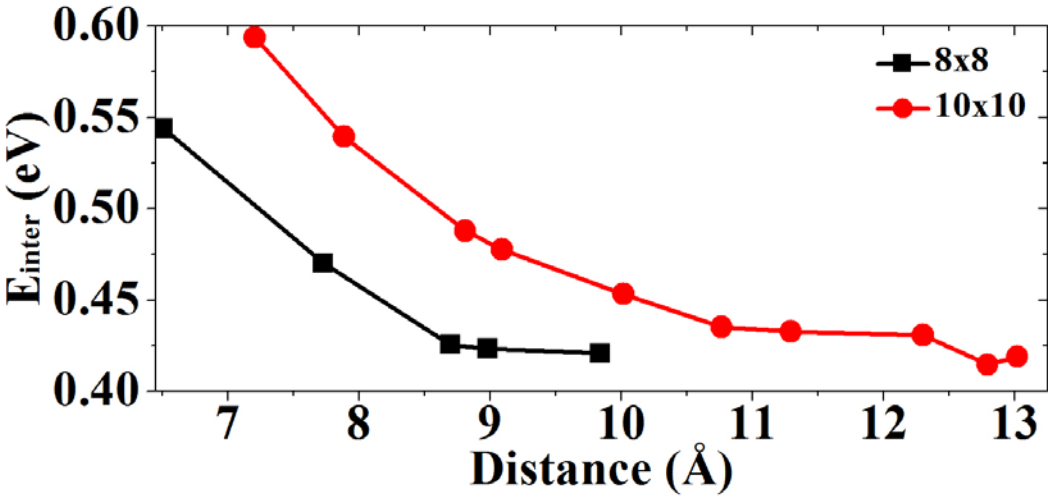

FIG. 4. Comparison of interaction energy between two K adatoms on 8×8 and 10×10 graphene. Graphene supercell with smaller size will have higher level of electron doping. Higher eletron doping level in the smaller supercell results in smaller interaction energy due to stronger electronic screening.

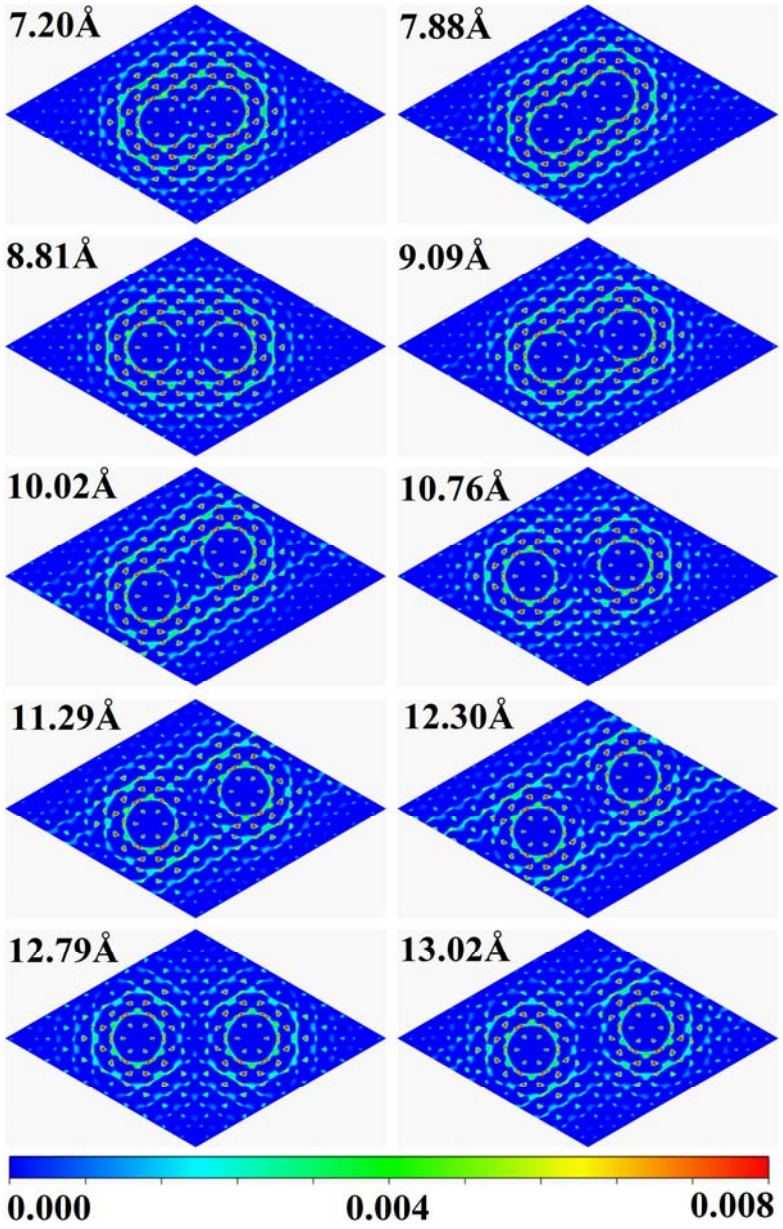

FIG. 5. Interaction charge density $\Delta\rho(r)$ for two K adatoms on graphene (color scale from 0.00 to 0.008 electrons/Å^3). $\Delta\rho(r)$ is found to be dependent on the separation distance and the orientation of the two adatoms relative to the graphene substrate.